Water Supply

Water Supply Vol 22 No 3, 2959 doi: 10.2166/ws.2021.420

Chlorophyll-a concentration inversion based on the modified Quasi-Analytical Algorithm and Sentinel-3 OLCI in Daihai Lake, China

Zhao Lu[a], Huajie Duan[b,*], Daqing Wang[a], Jianwu Cao[b], Guoli Du[b], Zhengdong Deng[a], Guangyuan Wang[a], Haoli Xu[a], Xiaoning Zhao[a] and Yue Shi[a]

[a] Army Engineering University of PLA, Nanjing 210007, China
[b] Research Institute for National Defence Engineering of PLA Academy of Military Science, Beijing 100850, China
*Corresponding author. E-mail: duanhuajie.2008@163.com

ABSTRACT

The Quasi-Analytical Algorithm (QAA) is effective in retrieving water inherent optical properties (IOPs) from remote sensing spectral reflectance and has wider applications in studies of the open ocean and coastal waters than of inland waters. This research aimed to modify the QAA model based on measured field spectral reflectance and absorption coefficients to render it applicable to studies of Daihai Lake, China. The improvements mainly included the reference wavelength selection, the power index of the particle backscattering coefficient and the exponential slope of the absorption coefficient of the colored detrital matter estimation. The average relative error between the inverse and measured absorption coefficients was less than 20%. A linear model was established between the phytoplankton absorption coefficient at a wavelength of 674 nm ($a_{ph}(674)$) and the chlorophyll-a (Chl-a) concentration, with a determination coefficient of 0.88. Additionally, the modified Quasi-Analytical Algorithm (MQAA) model was applied to the Ocean and Land Color Instrument (OLCI) data aboard the Sentinel-3 satellite. Finally, a spatial distribution map for the Chl-a concentrations in Daihai Lake on August 10, 2017, was drawn and the mid-eutrophication area was found to occur in the north and border.

Key words: chlorophyll-a, inherent optical properties, modified Quasi-Analytical Algorithm, remote sensing, Sentinel-3 OLCI

HIGHLIGHTS

- The quasi-analytical algorithm (QAA) is modified to MQAA.
- The MQAA is useful in application to OLCI data for chlorophyll-a concentration retrieval.
- The application of MQAA in Daihai is targeted.

INTRODUCTION

Water inherent optical properties (IOPs) mainly consist of the absorption coefficients of pure water $a_w(\lambda)$ (abbreviations are listed in Table 1), phytoplankton $a_{ph}(\lambda)$, non-algal particles $a_{nap}(\lambda)$, colored dissolved organic material $a_{CDOM}(\lambda)$, the backscattering coefficients of the pure water $b_{bw}(\lambda)$ and particulate matter $b_{bp}(\lambda)$, without the influence of external light. Therefore, accurate retrievals for the IOPs for the water constituent are essential for water quality inversion using remote sensing data.

To inverse the water IOPs from the remote sensing reflectance, semi-analytical algorithms based on the light radiation transfer principle have been put forward. These algorithms included the Shallow Water Inversion Model (SWIM) (McKinna *et al.* 2015), the Generalized Inherent Optical Properties (GIOP) (Werdell *et al.* 2013), Garver–Siegel–Maritorena Model (GSM) (Wang *et al.* 2016), and the Quasi-Analytical Algorithm (QAA) (Munnooru *et al.* 2019). Among these, the QAA model has the widest application for the study of ocean and coastal waters. The conversion relationship of the remote sensing reflectance above and below the water surface was constructed using the Hydrolight radiative transfer numerical model with consideration of the absorption and backscattering coefficients of the water constituent. The QAA model was first built and validated for multiband data (Lee *et al.* 2002), for example, Moderate Resolution Imaging Spectroradiometer (MODIS) and Sea-Viewing Wide Field-of-View Sensor (SeaWiFS) data for deep waters, then was applied to hyperspectral data and later

Table 1 | Summary of abbreviations for the parameters

Symbols	Definition	Unit
$a(\lambda)$	Total absorption coefficient	m^{-1}
$a_w(\lambda)$	Pure water absorption coefficient	m^{-1}
$a_{n\text{-}w}(\lambda)$	Non-water absorption coefficient, $a(\lambda)-a_w(\lambda)$	m^{-1}
$a_{ph}(\lambda)$	Phytoplankton absorption coefficient	m^{-1}
$a_p(\lambda)$	Particle absorption coefficient	m^{-1}
$a_{nap}(\lambda)$	Non-algal particle absorption coefficient	m^{-1}
$a_{CDOM}(\lambda)$	Colored dissolved organic material absorption coefficient	m^{-1}
$a_{CDM}(\lambda)$	Absorption coefficient of colored detrital matter, sum of the non-algal particles and the colored dissolved organic material, $a_{nap}(\lambda)+a_{CDOM}(\lambda)$	m^{-1}
$b_b(\lambda)$	Total backscattering coefficient	m^{-1}
$b_{bw}(\lambda)$	Pure water backscattering coefficient	m^{-1}
$b_{bp}(\lambda)$	Particle backscattering coefficient	m^{-1}
$R_{rs}(\lambda)$	Remote sensing reflectance above the water	sr^{-1}
$r_{rs}(\lambda)$	Remote sensing reflectance below the water	sr^{-1}
S_{CDM}	Exponential slope of the absorption coefficient of colored detrital matter	nm^{-1}
Y	Power index of the backscattering coefficient of the particles	–
$C_{Chl\text{-}a}$	Chlorophyll-a concentration	mg/m^3
λ	Wavelength	nm
λ_0	Reference wavelength	nm

extended to shallow waters (Barnes *et al.* 2017). The optical parameters that influence the model accuracy include the estimated absorption coefficient at the reference wavelength, the extrapolated backscattering coefficient of the particles, and the assumed absorption coefficient ratio for the specific wavelengths (Lee *et al.* 2010). Therefore, for lakes with specific water quality characteristics, the typical characteristic wavelength should be selected according to the satellite data source through the field measurement of spectral parameters to reduce the influence of uncertainty. In addition, some studies showed that the remote sensing data acquisition may also increase the uncertainty of the inversion model (Liuzzo *et al.* 2020). Before inversion, it is necessary to adopt appropriate methods to preprocess remote sensing data to reduce the errors caused by data acquisition.

The QAA algorithm has shown the advantages in reversion of inherent optical properties of water bodies; however, it requires specific bands, such as 413, 443, 490, 555, 640, 667, and 670 nm wavelengths, etc. The two wavelengths, 413 and 443 nm, are mainly used for total absorption coefficient decomposition for the phytoplankton pigment and CDM strong absorption, and the reflectance peak above the water surface is mostly near 555 nm. Most satellite sensors do not include the 413 nm wavelength for the atmosphere's strong absorbance of sunlight as being a weak receiving signal for the sensors. Thus, due to its requirement for specific wavelengths, the QAA algorithm is mainly applied to hyperspectral data measured on a water surface and medium spectral remote sensing data in MERIS, MODIS, Sea WIFS, etc.

In the past decade, the QAA model has been applied to inland water bodies such as the aquaculture ponds in Mississippi State (Mishra *et al.* 2014), the Great Lakes (Becker *et al.* 2009), and Liaohe River (Deng *et al.* 2019). However, as the spectral characteristic and the IOPs of inland waters are different from the open ocean and coastal waters, the QAA model still requires modifications before it can have wider applications. Huang *et al.* (2014a, 2014b) selected 710 nm as the reference wavelength in Poyang Lake and developed an optimization model after the spectral classification of four inland lakes in China. Yang *et al.* (2013) enhanced the spectral slope of the particles' backscattering coefficients and the chlorophyll-a (Chl-a) absorption coefficient at a wavelength of 443 nm. Li *et al.* (2013) chose 778 nm as the reference wavelength. Ma *et al.* (2006) calibrated the conversion coefficient of the remote sensing reflectance above and below the water surface in Taihu Lake. Pitarch *et al.* (2019) studied the effect of Raman scattering on QAA retrievals. Pitarch & Vanhellemont

(2021) presented the QAA-RGB, a universal three-band absorption and backscattering retrieval algorithm for high resolution satellite sensors. Thus far, no better progress has been made in customizing the QAA model for inland waters. Chlorophyll-a content in water is closely related to the eutrophication level and it shows spectral characteristics similar to terrestrial vegetation in remote sensing images. The spectral curve of chlorophyll-a shows absorption peaks in a blue wave segment and red band respectively, with a very prominent reflection peak in the near-infrared band which is obviously different from other components of water bodies. Previous studies on chlorophyll-a concentration have been carried out by using multi-source remote sensing data and integrating multiple methods, and the accuracy has been constantly improved. The remote sensing inversion methods for Chl-a concentrations can be broadly classified into two types: one type is the empirical model based on reflectivity, and the other type is the semi-analytical model based on absorption coefficient. The empirical models are based on band combinations, such as the double-band model (Pulliainen *et al.* 2001), three-band model (Bi *et al.* 2018), and four-band model (Shen *et al.* 2010). The semi-analytical models are based on the phytoplankton absorption coefficient. The relationship between the Chl-a concentration and the phytoplankton absorption coefficient for the power and linear (Sun *et al.* 2012) models varies in different inland waters.

In this study, the measured data including the in-situ remote sensing reflectance $R_{rs}(\lambda)$, the absorption coefficient of the non-water $a_{n\text{-}w}(\lambda)$, non-algal particles $a_{nap}(\lambda)$, and colored dissolved organic material $a_{CDOM}(\lambda)$, and the phytoplankton absorption coefficient $a_{ph}(\lambda)$ were employed to modify the QAA model for the inversion of the IOPs and Chl-a concentration for Daihai Lake. After applying the MQAA model to Sentinel-3 OLCI satellite data, the Chl-a concentration spatial distribution for August 10, 2017, was derived. The technical route of research is shown in Figure 1.

There are many parameters and symbols used in the study. In order to facilitate the understanding of the model method, the abbreviations of relevant parameters are explained in Table 1.

MATERIALS AND METHODS

Study area

Daihai Lake is located at 112°37′–112°46′E, 40°32′–40°37′N (Figure 2). It is a typical inland lake in a semi-arid area of Liangcheng County, Ulancha City, Inner Mongolia Autonomous Region, North China. The depth of the lake ranges from 4 to 16 m, with an average depth of 7 m. It is characterized as a light saltwater lake. The surface altitude is about 1,223 m and the average annual temperature is 5 °C. The water supply mainly depends on the intermittent rivers to the west, namely the Gongba River, Wuhao River, Buliang River, Tiancheng River and Muhua River. The icebound period lasts from late November to next April. In the past decades, the lake area has declined year by year due to low annual rainfall (427 mm) and high annual evaporation (1,938 mm).

Daihai Lake belongs to the Mengxin Lake System. Most of the lakes developed from relatively independent inland basin water systems. Under arid and semi-arid climate conditions, strong solar irradiation and scarce rainfall supplement,

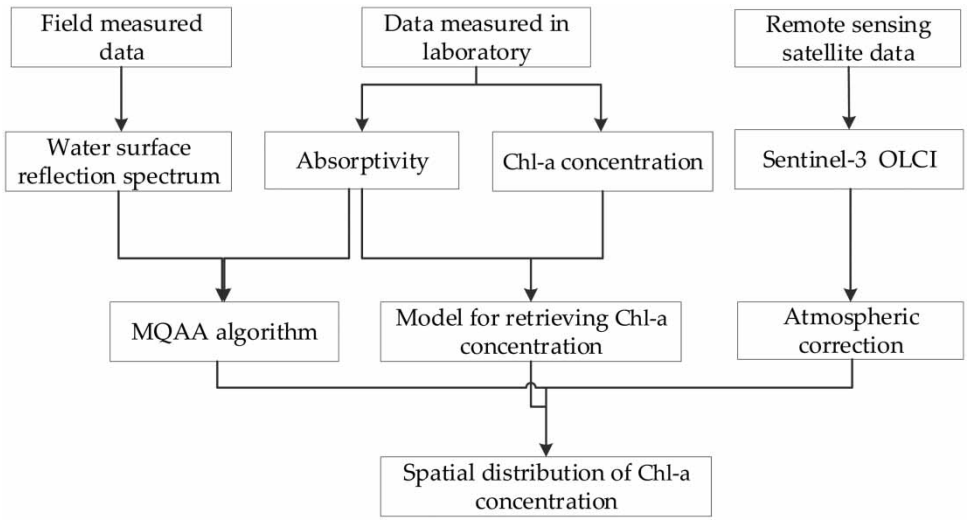

Figure 1 | Technical route of retrieving chlorophyll-a concentration by remote sensing.

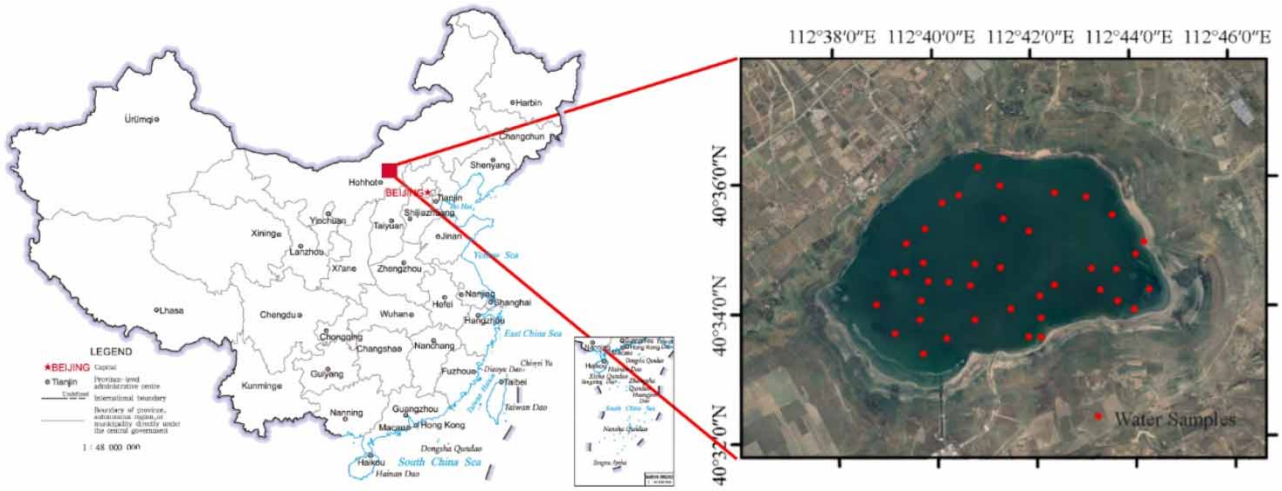

Figure 2 | The location of the water sample points.

coupled with vigorous evaporation, have made the Daihai Lake water supply of the river system exceed its income, resulting in degradation (Liang *et al.* 2017). In addition, reclamation activities such as vegetation destruction and inappropriate grassland protection, as well as the utilization of supplementary water resources, have seriously damaged the water and salt balance under normal conditions, resulting in salinity (Xi *et al.* 2012). The discharge of industrial wastewater, domestic sewage, farmland drainage, etc., leads to organic pollutants entering Daihai Lake water bodies and being enriched, which can lead to serious eutrophication (Zeng & Wu 2010). In the last 20 years, the water pollution in Daihai Lake have been serious, and the concentrations of COD_{Mn}, BOD_5 and TP have exceeded the standard to varying degrees (Liang *et al.* 2021). The water quality in Daihai Lake is alkaline, and the degree of alkalization is still increasing (Zhou *et al.* 2006).

Data sources

According to the characteristics of water quality change and satellite transit time, a field survey and water sample collection were conducted in Daihai Lake on August 10, 2017, from 10:00 am to 12:00 pm. The actual sampling points are selected according to the principle of uniform distribution in the region and obvious difference in water quality characteristics. A total of 40 water samples were selected. The spectral reflectance of the water surface at the water sample points was collected by ASD Field Handheld 2 spectrometer, and the water about 10 cm below the water surface was collected by sampling bottle. The collected water was sealed and stored in dark bottles, and the absorption coefficient and Chl-a concentration of water samples were determined under laboratory conditions. To reduce the error, the reflectivity of each sampling point was collected five times, and the average value of the reflectivity was taken as the reflectivity. Five groups of water samples were also collected at each sampling point, and the measured average Chl-a concentration was taken as the Chl-a concentration at the sampling point. The distribution of sampling points is shown in Figure 2.

The above-water measurement method was employed using an azimuth angle of 135° and an elevation angle of 40° to avoid the influence of mirror reflections from the water and the diffuse light scattering from the sky. The measured radiances included the water ($L_{sw}(\lambda)$, W/(m^2.nm.sr)), the diffuse light scattering from the sky ($L_{sky}(\lambda)$, W/(m^2.nm.sr)), and the standard white board ($L_p(\lambda)$, W/(m^2.nm.sr)) with a reflectance (ρ_p) of 100% using an ASD Field Handheld 2 spectrometer with a wavelength range of 325–1,075 nm and a 1 nm interval. The reflectance on the air–water interface (r) was taken as 0.025 using the 5 m/s wind-speed conditions determined on-site. The remote sensing reflectance above the water ($R_{rs}(\lambda)$, Figure 3) was calculated as follows (Tang *et al.* 2004):

$$R_{rs}(\lambda) = \frac{\rho_p(L_{sw}(\lambda) - rL_{sky}(\lambda))}{L_p(\lambda)\pi} \quad (1)$$

The acetone method and ethanol method were the main methods for extracting Chl-a (Chen & Gao 2000). Spectrophotometry (Lorenzen 1967) and fluorescence (Yentsch & Menzel 1963) were the two main methods for the determination

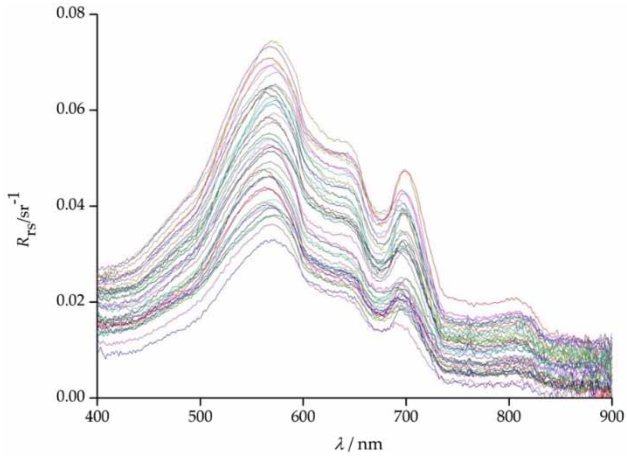

Figure 3 | Above-water surface remote sensing reflectance $R_{rs}(\lambda)$.

of Chl-a. *Water Quality – Determination of Chl-a – Spectrophotometric Method* (HJ897-2017) is a standard document formulated by the Ministry of Ecology and Environment of the People's Republic of China. This document regulates the determination of Chl-a, and can be downloaded from the website http://www.mee.gov.cn/ywgz/fgbz/bz/bzwb/jcffbz/201712/t20171227_428728.shtml. In the study, Chl-a concentrations were determined according to the requirements of this standard. The water samples were filtered through GF/F membranes, and then frozen for 48 h at −20 °C. After chlorophyll extraction by acetone, the absorbance of the membrane and acetone were measured at wavelengths of 665 and 750 nm, respectively, using a TU-1810 ultraviolet–visible spectrophotometer and then twice after a drop of 1% hydrochloric acid (Clevers & Gitelson 2013). Then the Chl-a concentrations were measured by spectrophotometry.

The absorbances of the non-water ($OD_{n\text{-}w}(\lambda)$), non-algal particles ($OD_{nap}(\lambda)$), and the colored dissolved organic material ($OD_{CDOM}(\lambda)$) were measured using a TU-1810 ultraviolet–visible spectrophotometer. With pure water as the baseline, the absorbances of the water samples before and after filtration were measured and labeled as non-water and colored dissolved organic material, respectively. The absorption coefficients of the non-algal particles were derived using the quantitative filter technique. After extraction by ethanol, the absorbance of the filtered GF/F membrane was measured as the non-algal particles. The corresponding absorption coefficients were obtained from the absorbances as follows:

$$a_{n\text{-}w}(\lambda) = 2.303 OD_{n\text{-}w}(\lambda)/L \tag{2}$$

$$a_{nap}(\lambda) = 2.303 OD_{nap}(\lambda) S/V \tag{3}$$

$$a_{CDOM}(\lambda) = 2.303 OD_{CDOM}(\lambda)/L \tag{4}$$

where L (m), S (m^2), and V (m^3) represent the optical path with a value of 0.01, the membrane filter area, and water sample volume, respectively; $a_{n\text{-}w}(\lambda)$ represents the absorption coefficients of non-water; $a_{nap}(\lambda)$ represents the absorption coefficients of non-algal particles; and $a_{CDOM}(\lambda)$ represents the absorption coefficients of colored dissolved organic material.

After adding $a_{nap}(\lambda)$ and $a_{CDOM}(\lambda)$, the $a_{CDM}(\lambda)$ was derived as shown in Figure 4. Finally, the $a_{ph}(\lambda)$ (Figure 5) was obtained by subtracting $a_{CDM}(\lambda)$ from $a_{n\text{-}w}(\lambda)$ (Figure 6).

The Sentinel-3 satellite carrying the 21-band OLCI sensor (Table 2) with a spatial resolution 300 m was launched in February 2016. The satellite was intended as a substitute for the Medium-Spectral Resolution Imaging Spectrometer (MERIS) for the purpose of land and ocean observation (Zhang *et al.* 2009). The Sentinel-3 OLCI data from August 10, 2017, were downloaded from the website https://sentinel.esa.int/web/sentinel/missions/sentinel-3. To reduce the inversion error caused by remote sensing data, the data were preprocessed for geometric positioning, calibration, and atmospheric corrections using the Fast Line-of-sight Atmospheric Analysis of Hypercubes (FLAASH) model and a resampled spatial resolution of 30 m.

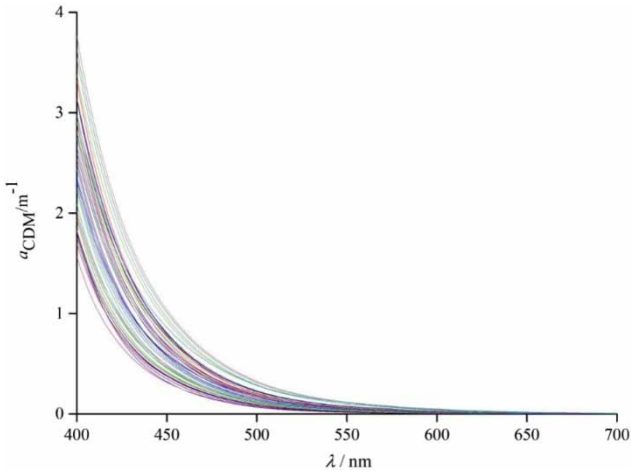

Figure 4 | Measured absorption coefficients of the colored detrital particles $a_{CDM}(\lambda)$.

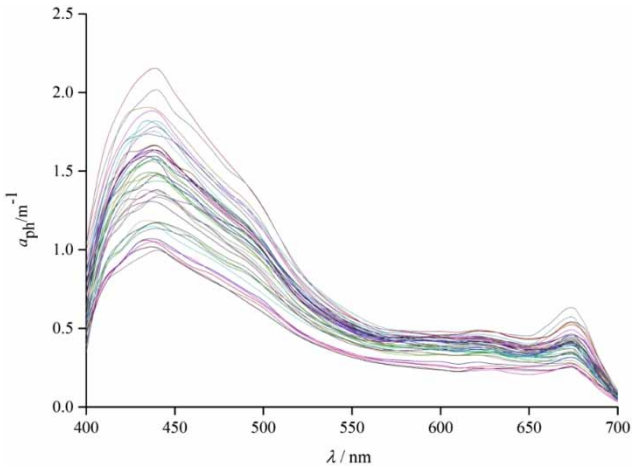

Figure 5 | Measured phytoplankton absorption coefficients $a_{ph}(\lambda)$.

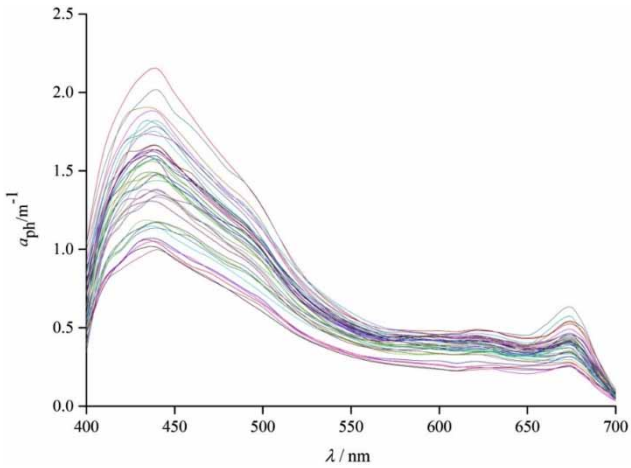

Figure 6 | Measured non-water absorption coefficients $a_{n\text{-}w}(\lambda)$.

Table 2 | The bands on the Sentinel-3 OLCI sensor

Band number	Center wavelength/nm	Bandwidth/nm	Spatial resolution/m
1	400	15	300
2	412.5	10	
3	443	10	
4	490	10	
5	510	10	
6	560	10	
7	620	10	
8	665	10	
9	673.75	7.5	
10	681	7.5	
11	709	10	
12	754	7.5	
13	761	2.5	
14	764.375	3.75	
15	767.5	2.5	
16	779	15	
17	865	20	
18	885	10	
19	900	10	
20	940	20	
21	1,020	40	

QAA model

The QAA algorithm was proposed based on the radiation transmission model of a water body and it is applied to the optical deep-water area with several improvements and modifications. The basic idea of this algorithm is to establish the quantitative relationship between the remote sensing reflectivity and inherent optical quantity of the water body. Firstly, the total absorption coefficient of the effluent body is retrieved, and the reflectance of the water surface is calculated from the reflectance above the water surface. Then the total absorption coefficient of the water body at the reference band is determined by the empirical inversion model, and the total backscattering coefficient at the reference wavelength is obtained. Combined with the empirical values of the power exponent, the backscattering coefficient at full wavelength is obtained, and then the total absorption coefficient at full wavelength is inversely derived. Based on the above, the total absorption coefficient decomposition was carried out. The phytoplankton pigment absorption coefficient ratio between 413 and 443 nm was estimated by the empirical formula. With the measured CDM absorption coefficient, the slope index was fitted out. After solving the total absorption coefficient equations, the absorption coefficients for phytoplankton pigment and CDM at the wavelengths 413 and 443 nm were derived. On the basis of slope index, the CDM absorption coefficient at other wavelengths can be extrapolated. Finally, the phytoplankton pigment absorption coefficient at all wavelengths can be obtained.

The basic steps of the QAA algorithm are divided into 12 steps, consisting of the three-step half-analysis relationship, four-step analysis relationship and five-step empirical relationship, which can be applied to the measured hyperspectral water surface and spectral data in multiple categories on board.

The bio-optical model served as the basis for the QAA model mainly used for determining the absorption coefficients $a(\lambda)$ and backscattering coefficients $b_b(\lambda)$ of the water components as shown below:

$$a(\lambda) = a_w(\lambda) + a_{ph}(\lambda) + a_{CDM}(\lambda) \tag{5}$$

$$b_b(\lambda) = b_{bw}(\lambda) + b_{bp}(\lambda) \tag{6}$$

The above-water reflectance $R_{rs}(\lambda)$ was converted to the subsurface reflectance $r_{rs}(\lambda)$ empirically using the equation below:

$$r_{rs}(\lambda) = \frac{R_{rs}(\lambda)}{0.52 + 1.7R_{rs}(\lambda)} \tag{7}$$

The dependence of the subsurface reflectance $r_{rs}(\lambda)$ on the total absorption $a(\lambda)$ and backscattering coefficient $b_b(\lambda)$ based on the mechanism analysis is shown below:

$$u(\lambda) = \frac{b_b(\lambda)}{a(\lambda) + b_b(\lambda)} \tag{8}$$

$$r_{rs}(\lambda) = g_0 u(\lambda) + g_1 [u(\lambda)]^2 \tag{9}$$

where the values of g_0 and g_1 were 0.0895 and 0.1247, respectively.

The relationship between the backscattering coefficient $b_b(\lambda)$ and the wavelength was in accordance with the power function with Y as the unknown as follows:

$$b_{bp}(\lambda) = b_{bp}(\lambda_0)\left(\frac{\lambda_0}{\lambda}\right)^Y \tag{10}$$

For the absorption coefficient decomposition, two variables, namely the ratios of the absorption coefficients at wavelengths of 413 and 443 nm, respectively for the phytoplankton and the colored detrital particles were introduced as follows:

$$\beta = \frac{a_{ph}(413)}{a_{ph}(443)} \tag{11}$$

$$\eta = \frac{a_{CDM}(413)}{a_{CDM}(443)} \tag{12}$$

The two variables were expressed with the undetermined $S_{CDM}(\lambda)$ as the equations:

$$\beta = 0.71 + \frac{0.06}{0.8 + r_{rs}(443)/r_{rs}(560)} \tag{13}$$

$$\eta = e^{S_{CDM}(443-413)} \tag{14}$$

The absorption coefficient of the colored detrital material $a_{CDM}(\lambda)$ declines in exponent regularity with the wavelength as follows:

$$a_{CDM}(\lambda) = a_{CDM}(443)e^{S_{CDM}(443-\lambda)} \tag{15}$$

MQAA model

Based on the QAA model and the measured $a_{n\text{-}w}(\lambda)$, $a_{CDM}(\lambda)$, $a_{ph}(\lambda)$, the reference wavelength was reselected and the linear fitting models for the Y and S_{CDM} estimation were established.

The difference between the absorption coefficients of pure water and the water samples provides the basis for estimating the total absorption coefficient and this difference was quite small at near-infrared wavelengths. Based on the measurement comparison, the reference wavelength was chosen as 710 nm, close to the band 11 wavelength on the Sentinel-3 OLCI, where the $a_{n\text{-}w}$ was approximate to zero (Figure 6).

The power function index of the particle backscattering coefficient varies in water samples due to the different compositions and sizes of the particles and this influences the inversion result (Gallegos *et al.* 2005; Wang *et al.* 2017). Y can be estimated by empirical relation to the subsurface reflectance ratio of the blue and green bands (Aurin & Dierssen 2012) and varies depending on the reference wavelength (Yang *et al.* 2013). The particle backscattering coefficient was calculated

with the measured spectral reflectance and the non-water absorption coefficient (Figure 7). After the power function fitting, the indices for the 40 samples were derived with one fitting example as shown in Figure 8 and were in the range 0.99–2.65 (Figure 9). The linear model was built between Y and the subsurface reflectance ratio at wavelengths of 440 and 560 nm (Figure 10).

After fitting the absorption coefficient of the colored detrital materials for the 40 water samples with the one fitted example shown in Figure 11, the obtained exponential slopes were in the range 0.019–0.037 (Figure 12) and elucidated the linear relationship with the ratio of the subsurface reflectance at the wavelengths of 440 and 560 nm (Figure 13).

Combining the QAA model and the above improvement, we obtained a concrete process for the MQAA model (Table 3).

Assessment of the retrieved result

The retrieved accuracy can be evaluated by statistical indices; and the root mean square error (RMSE), the average relative error (ARE), and the coefficient of determination (R^2) are as follows:

$$RMSE = \sqrt{\frac{\sum_{i=1}^{N} (X_{\text{est},i} - X_{\text{mea},i})^2}{N}} \tag{16}$$

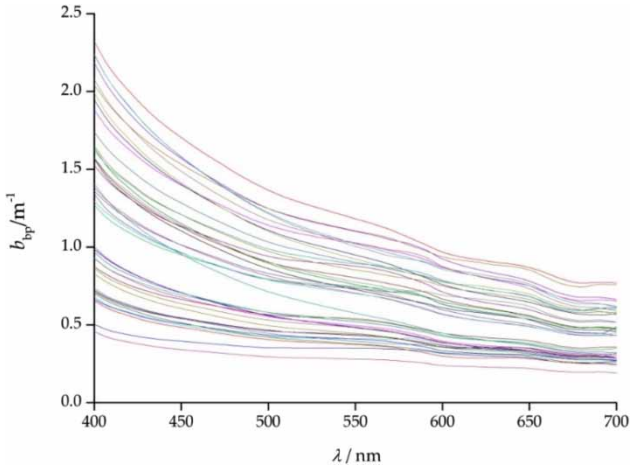

Figure 7 | The retrieved particle backscattering coefficients $b_{bp}(\lambda)$.

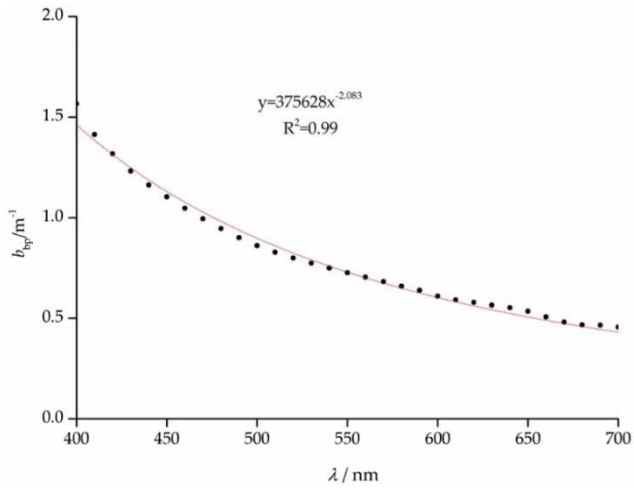

Figure 8 | The power function fitting of particle backscattering coefficient b_{bp} for water sample 1.

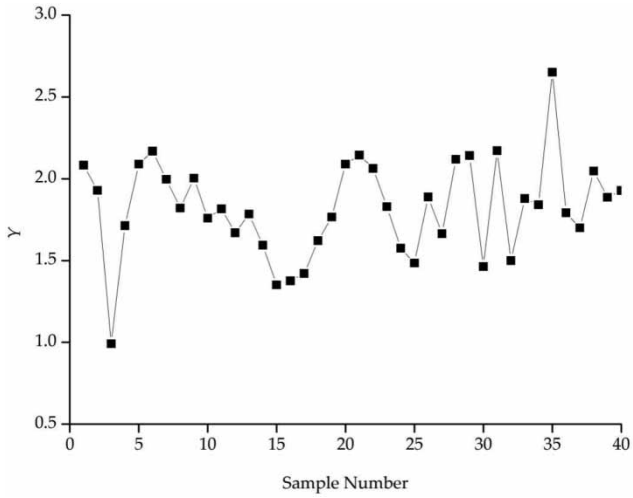

Figure 9 | The fitting power index of the backscattering coefficient of the particles *Y* values based on the power function.

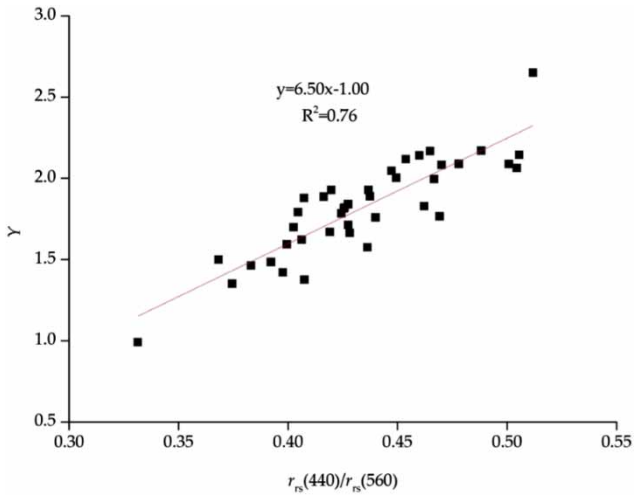

Figure 10 | The linear model between the power index of the backscattering coefficient of the particles *Y* and the subsurface reflectance ratio at wavelengths of 440 and 560 nm.

$$ARE = \frac{1}{N}\sum_{i=1}^{N}\frac{|X_{\mathrm{est},i} - X_{\mathrm{mea},i}|}{X_{\mathrm{mea},i}} \tag{17}$$

where N is the number of the water samples; $X_{\mathrm{est},i}$ is the estimated value; and $X_{\mathrm{mea},i}$ is the measured value.

RESULTS AND DISCUSSION

Remote sensing spectra

From the measured above-water remote sensing reflectance curve, we found three main peaks in the ranges of 560–570, 690–700, and 800–810 nm and an obvious trough at 670–680 nm (Yang *et al.* 2013). The first and third peaks were mainly caused by the strong reflection of the particles, while the second was caused by the typical reflection characteristics of Chl-a. The typical absorption of the Chl-a produced the trough and the reflection of wavelengths in the range 400–500 nm was low due to the water composition absorption (Sun *et al.* 2012).

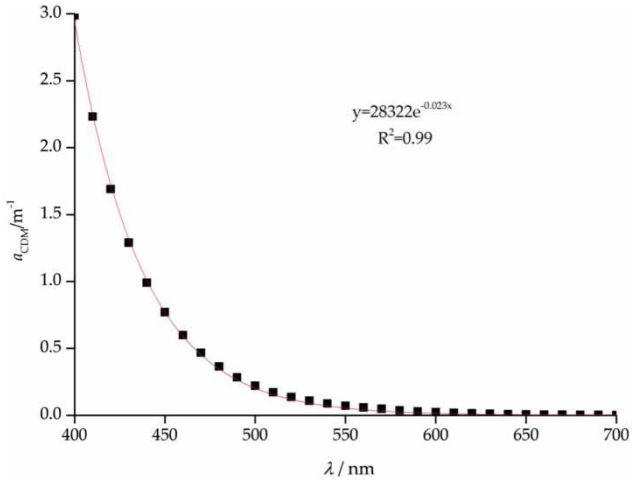

Figure 11 | The exponential function fitting of exponential slope of the absorption coefficient of the colored detrital matter S_{CDM} for water sample 1.

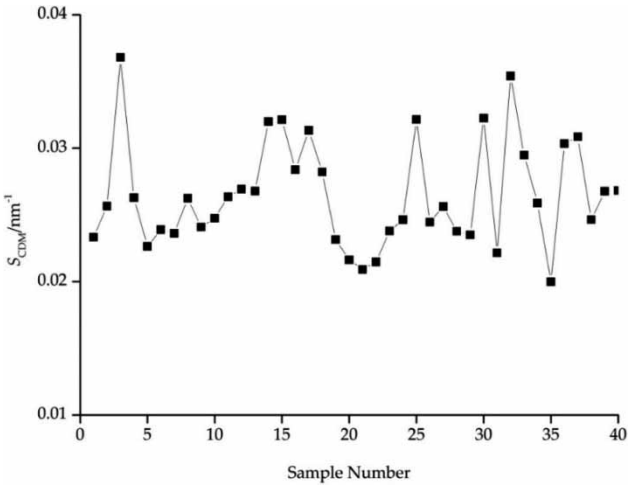

Figure 12 | The fitting exponential slope of the absorption coefficient of the colored detrital matter S_{CDM} values based on the exponential function.

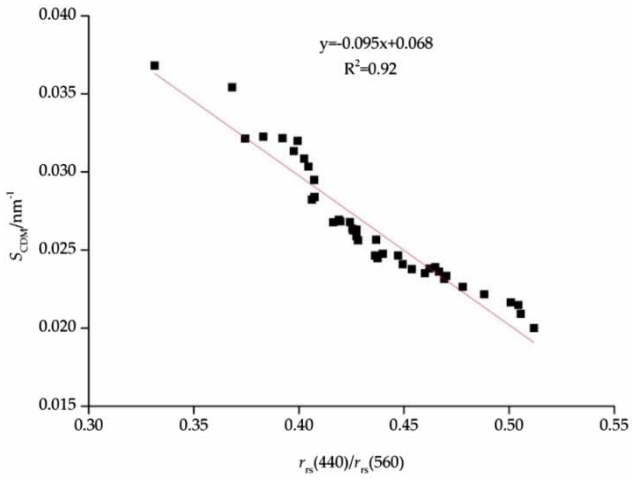

Figure 13 | The linear model between S_{CDM} and the subsurface reflectance ratio at wavelengths of 440 and 560 nm.

Table 3 | Flow of the MQAA

Steps	Properties	Equation	Approach
Step 0	$r_{rs}(\lambda)$	$= R_{rs}(\lambda)/(0.52 + 1.7R_{rs}(\lambda))$	Semi-analytical
Step 1	$u(\lambda)$	$= \frac{-g_0 + \sqrt{(g_0)^2 + 4g_1 r_{rs}(\lambda)}}{2g_1}$, $g_0 = 0.0895$, $g_1 = 0.1247$	Semi-analytical
Step 2	$a(710)$	$= a_w(710)$	Empirical
Step 3	$b_{bp}(710)$	$= \frac{u(710)a(710)}{1 - u(710)} - b_{bw}(710)$	Analytical
Step 4	Y	$= 6.50 r_{rs}(440)/r_{rs}(560) - 1.00$	Empirical
Step 5	$b_{bp}(\lambda)$	$= b_{bp}(710)(710/\lambda)^Y$	Semi-analytical
Step 6	$a(\lambda)$	$= \frac{[1 - u(\lambda)][b_{bw}(\lambda) + b_{bp}(\lambda)]}{u(\lambda)}$	Analytical
Step 7	S_{CDM}	$= -0.095 r_{rs}(440)/r_{rs}(560) + 0.068$	Empirical
Step 8	β, η	$\beta = 0.71 + \frac{0.06}{0.8 + r_{rs}(443)/r_{rs}(560)}$, $\eta = e^{S_{CDM}(443-413)}$	Empirical
Step 9	$a_{CDM}(443)$	$= \frac{[a(413) - \beta a(443)] - [a_w(413) - \beta a_w(443)]}{\eta - \beta}$	Analytical
Step 10	$a_{CDM}(\lambda)$	$= a_{CDM}(443) e^{S_{CDM}(443-\lambda)}$	Empirical
Step 11	$a_{ph}(\lambda)$	$= a(\lambda) - a_w(\lambda) - a_{CDM}(\lambda)$	Analytical

Comparison of the inversed and measured absorption coefficient

In order to analyze the inversion precision of the MQAA model, five characteristic wavelengths, 400, 410, 440, 560, and 674 nm, respectively, were chosen and the three statistical indices, RMSE, R^2, and ARE were used to evaluate the inversion error for the absorption coefficients. Between the inversed and measured $a_{n\text{-}w}$ (Figure 14), the RMSE was in the range 0.026–0.167, with an R^2 value above 0.90, and an ARE of no more than 16% (Table 4). For the a_{CDM} (Figure 15), the RMSE was below 0.20, R^2 was above 0.98, and the ARE varied in the range 4%–20% (Table 5). With regard to the a_{ph} (Figure 16), the inversion performed well with an RMSE below 0.14, R^2 above 0.90, and ARE in the range 4%–16% (Table 6), providing support for the Chl-a concentration estimation. The result showed the inversion accuracy satisfied the research requirement.

Chl-a concentration inversion based on the phytoplankton absorption coefficient

The measured Chl-a concentration showed a linear relationship with the measured phytoplankton absorption coefficient at a wavelength of 674 nm, an R^2 of 0.88 (Figure 17), and with the inversed $a_{ph}(674)$, an R^2 of 0.87 (Figure 18).

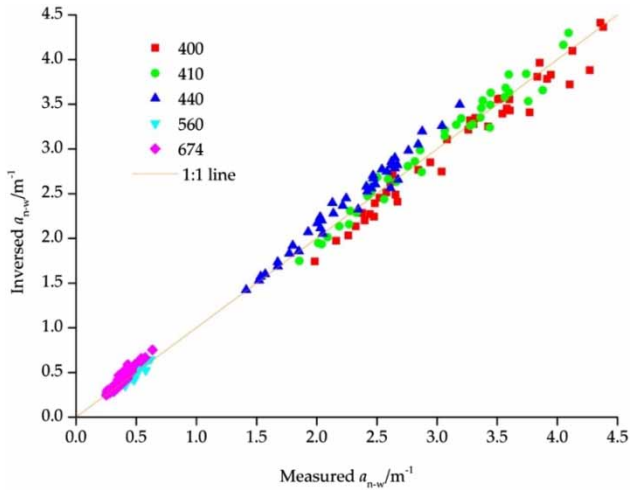

Figure 14 | The comparison of the inversed and measured $a_{n\text{-}w}$ in different wavelengths.

Table 4 | RMSE, R^2 and ARE of the inversed and measured $a_{n\text{-}w}$

	RMSE	R^2	ARE
$a_{n\text{-}w}(400)$	0.167	0.968	4.47%
$a_{n\text{-}w}(410)$	0.119	0.970	3.40%
$a_{n\text{-}w}(440)$	0.165	0.977	5.76%
$a_{n\text{-}w}(560)$	0.026	0.943	4.32%
$a_{n\text{-}w}(674)$	0.077	0.910	15.23%

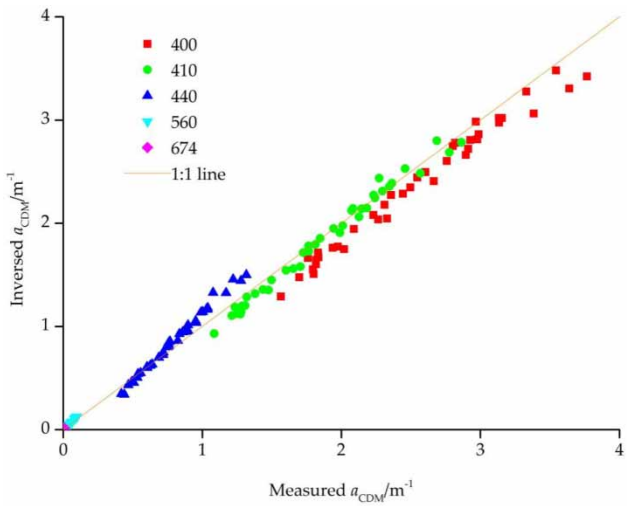

Figure 15 | The comparison of the inversed and measured a_{CDM} in different wavelengths.

Table 5 | RMSE, R^2 and ARE of the inversed and measured a_{CDM}

	RMSE	R^2	ARE
$a_{CDM}(400)$	0.191	0.981	7.34%
$a_{CDM}(410)$	0.081	0.987	4.13%
$a_{CDM}(440)$	0.100	0.993	9.05%
$a_{CDM}(560)$	0.011	0.995	19.10%
$a_{CDM}(674)$	0.001	0.983	19.20%

Chl-a concentration inversion by Sentinel-3 OLCI

The wavelengths in the MQAA model were replaced by the matched bands in the Sentinel-3 OLCI data. The MQAA model was applied to the preprocessed Sentinel-3 OLCI data to inverse the phytoplankton absorption coefficient and the linear regression model is shown in Figure 19 with an R^2 of 0.84, less than the inversion precision based on the measured $a_{ph}(674)$ for the estimation error.

The space distribution of the Chl-a concentrations in Daihai Lake on August 10, 2017, were drawn after applying the MQAA model to the entire area (Figure 20).

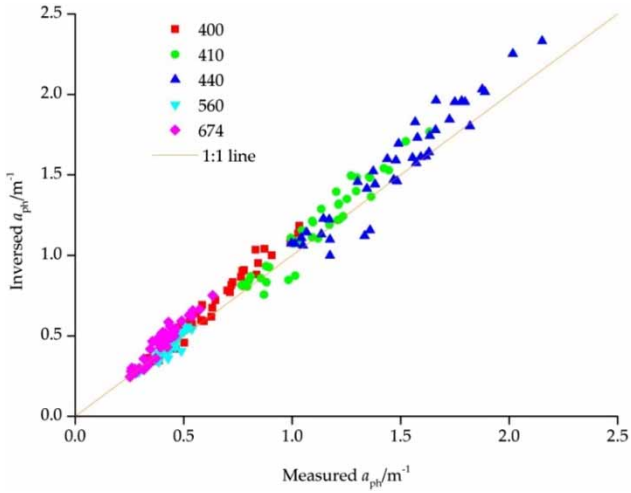

Figure 16 | The comparison of the inversed and measured a_{ph} in different wavelengths.

Table 6 | RMSE, R^2 and ARE of the inversed and measured a_{ph}

	RMSE	R^2	ARE
$a_{ph}(400)$	0.083	0.964	10.51%
$a_{ph}(410)$	0.103	0.928	7.44%
$a_{ph}(440)$	0.136	0.916	7.43%
$a_{ph}(560)$	0.026	0.900	4.32%
$a_{ph}(674)$	0.077	0.911	15.27%

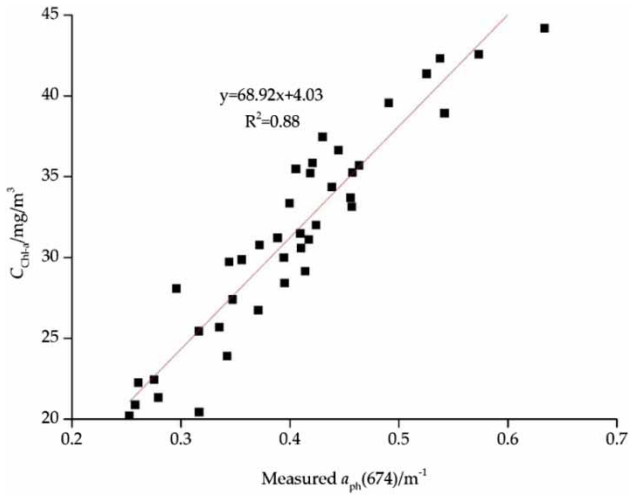

Figure 17 | Linear fitting model between $C_{Chl\text{-}a}$ and measured a_{ph} (674).

Based on the relationship between the eutrophication level index (TLI) and $C_{Chl\text{-}a}$, light eutrophication occurs at $C_{Chl\text{-}a}$ values in the range 10–25 mg/m^3, while middle eutrophication occurs in the range 25–60 mg/m^3 (Aurin & Dierssen 2012), and the TLI formula is expressed as follows:

$$TLI(\text{Chl-a}) = 10(2.5 + 1.086 \ln C_{\text{Chl-a}}) \quad (18)$$

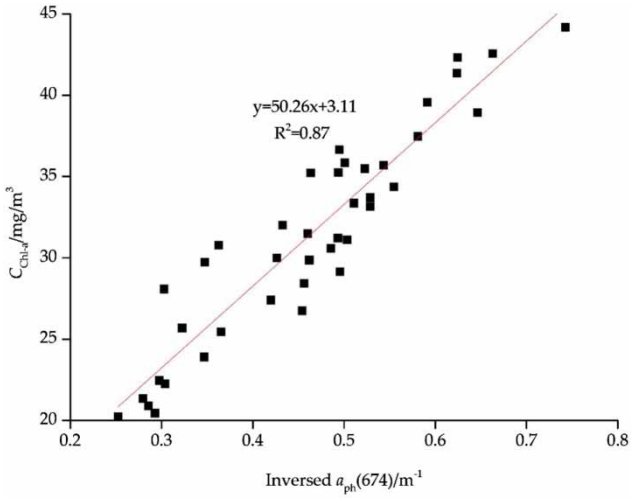

Figure 18 | Linear fitting model between $C_{Chl\text{-}a}$ and inversed a_{ph} (674).

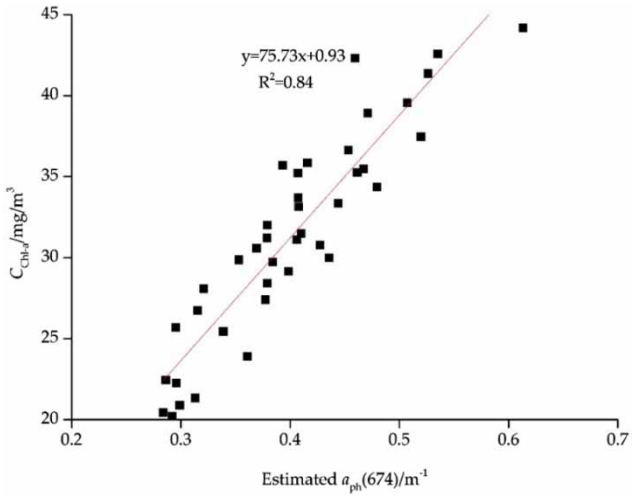

Figure 19 | Linear fitting model between $C_{Chl\text{-}a}$ and a_{ph}(674) based on Sentinel 3 OLCI.

We observed an increasing trend in the Chl-a concentrations from south to north, and mid-eutrophication occurred in the north and outermost edge at an area proportion of 84% (Table 7). The main reasons for this feature of the distribution map are the human activity at the edge and tourism development in the north.

CONCLUSIONS

In this study, the MQAA model was put forward on the basis of the measured data including the in-situ remote sensing reflectance, the absorption coefficient of the non-water, colored dissolved material, phytoplankton, and the Chl-a concentration to inverse the IOPs and Chl-a concentrations in Daihai Lake. From these results, we can draw certain conclusions as follows.

(1) The 710 nm wavelength in close proximity to band 11 on the Sentinel-3 OLCI was suitable as the reference wavelength, where the absorption coefficient was dominated by pure water absorption.
(2) Based on the measured $a_{n\text{-}w}$ and R_{rs} values, the backscattering coefficients for the particles were derived and the power function index Y was fitted and elucidated the linear relationship between the subsurface reflectance ratio at wavelengths of 440 and 560 nm with an R^2 of 0.76.

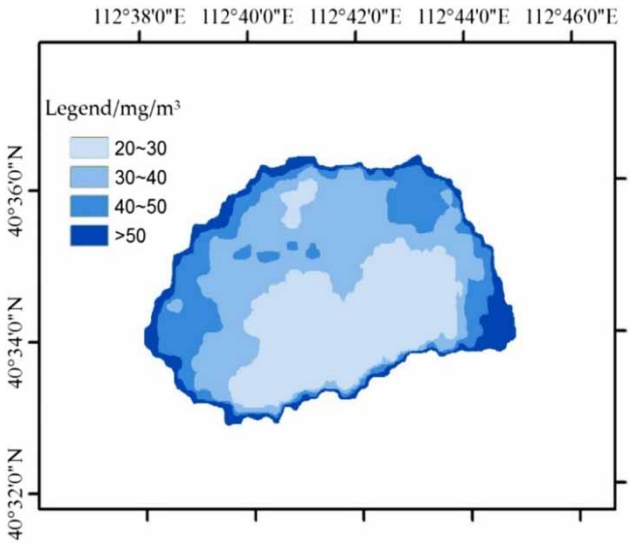

Figure 20 | The space distribution of the Chl-a concentration in Daihai Lake on August 10, 2017.

Table 7 | The area proportion of the $C_{Chl\text{-}a}$ gradient

$C_{Chl\text{-}a}$ (mg/m³)	20–30	30–40	40–50	50–60
Proportion (%)	31.84%	37.62%	22.86%	7.67%

(3) The exponential slopes were obtained after fitting a_{CDM} and performing the linear fitting relationship with the ratio of $r_{rs}(440)$ and $r_{rs}(560)$ with an R^2 of 0.92.
(4) After comparing the inversed and measured absorption coefficients at the five characteristic wavelengths of 400 nm, 410 nm, 440 nm, 560 nm, 674 nm, respectively, the range for the three statistical indices, RMSE, R^2, and ARE were below 0.20, above 0.90, and no more than 20%, respectively.
(5) The measured $C_{Chl\text{-}a}$ and $a_{ph}(674)$ showed a linear relationship with an R^2 of 0.88 and the MQAA model was applied to the preprocessed Sentinel-3 OLCI data for Daihai Lake. The delineated space distribution of the Chl-a concentrations revealed an increasing trend from south to north, and the mid-eutrophication occurred in the north and the outermost edge at an area proportion of 84%.

The results of this study filled the gap of using a semi-analytical model to retrieve water quality in semi-arid lakes, improved the accuracy of remote sensing retrieval of inland lake water quality, and provided support for the detection of inland water characteristic changes. The model proposed in the study was suitable for Daihai Lake. In the follow-up study, the model can also be applied to the inversion of suspended solids, salinity and other water parameters, so as to master the water quality of Daihai Lake more comprehensively. It should be noted that, although the model has a good effect in water quality inversion in Daihai Lake, its applicability in other similar salt lakes is still worth studying. In addition, there may be differences in water quality in different periods. In order to understand the water quality in Daihai Lake more comprehensively, it is necessary to obtain more Sentinel-3 OLCI data to analyze its temporal and spatial variation characteristics. The low spatial resolution of Sentinel-3 OLCI data also limits the application potential of this model to some extent. In order to enhance the applicability of the model, it is necessary to explore the inversion effect of the model based on other multispectral remote sensing data with higher spatial resolution.

CONFLICTS OF INTEREST

The authors declare no conflict of interest. The founding sponsors had no role in the design of the study; in the collection, analyses, or interpretation of data; in the writing of the manuscript, and in the decision to publish the results.

FUNDING

This work was supported by Military Research Project: Research on the Key Technology for Water Source Detection System Based on Remote Sensing Information and Development Program of China: Groundwater Exploration Technology in the Water Shortage Region (863 Program: 2012AA062601).

DATA AVAILABILITY STATEMENT

All relevant data are included in the paper or its Supplementary Information.

REFERENCES

Aurin, D. A. & Dierssen, H. M. 2012 Advantages and limitations of ocean color remote sensing in CDOM-dominated, mineral-rich coastal and estuarine waters. *Remote Sensing of Environment* **125**, 181–197. doi:10.1016/j.rse.2012.07.001.

Barnes, B. B., Garcia, R., Hu, C. & Lee, Z. 2017 Multi-band spectral matching inversion algorithm to derive water column properties in optically shallow waters: an optimization of parameterization. *Remote Sensing of Environment* **204**, 424–438. doi:10.1016/j.rse.2017.10.-013.

Becker, R. H., Sultan, M. I., Boyer, G. L., Twiss, M. R. & Konopko, E. 2009 Mapping cyanobacterial blooms in the Great Lakes using MODIS. *Journal of Great Lakes Research* **35** (3), 447–453. doi:10.1016/j.jglr.2009.05.007.

Bi, S., Li, Y., Lv, H., Zhu, L., Mu, M., Lei, S., Xu, J., Wen, S. & Ding, X. 2018 Estimation of chlorophyll-a concentration in Lake Erhai based on OLCI data. *Journal of Lake Sciences* **30** (3), 701–712. doi:10.18307/2018.0312.

Chen, Y. W. & Gao, X. Y. 2000 Comparison of two methods for phytoplankton chlorophyll-a concentration measurement. *Journal of Lake Sciences* **12** (2), 185–188. doi:10.18307/2000.0215.

Clevers, J. G. P. W. & Gitelson, A. A. 2013 Remote estimation of crop and grass chlorophyll and nitrogen content using red-edge bands on Sentinel-2 and -3. *International Journal of Applied Earth Observation and Geoinformation* **23**, 344–351. doi:10.1016/j.jag.2012.10.008.

Deng, Z., Sun, Y., Qiu, Q., Ni, P. & Xing, R. 2019 Monitoring the suspended sediment concentration of Liaohe River delta using Tiangong-2 image based on quasi-analytical algorithm. *Journal of Capital Normal University (Natural Science Edition)* **40** (6), 75–82. doi:10.19789/j.1004-9398.2019.06.016.

Gallegos, C. L., Jordan, T. E., Hines, A. H. & Weller, D. E. 2005 Temporal variability of optical properties in a shallow, eutrophic estuary: seasonal and interannual variability. *Estuarine, Coastal and Shelf Science* **64** (2–3), 156–170. doi:10.1016/j.ecss.2005.01.013.

Huang, C., Li, Y., Yang, H., Li, J., Chen, X., Sun, D., Le, C., Zou, J. & Xu, L. 2014a Assessment of water constituents in highly turbid productive water by optimization bio-optical retrieval model after optical classification. *Journal of Hydrology* **519** (B), 1572–1583. doi:10.1016/j.jhydrol.2014.09.007.

Huang, J., Chen, L., Chen, X., Tian, X., Feng, L., Yesou, H. & Li, F. 2014b Modification and validation of a quasi-analytical algorithm for inherent optical properties in the turbid waters of Poyang Lake, China. *Journal of Applied Remote Sensing* **8** (1), 083643. doi:10.1117/1.JRS.8.083643.

Lee, Z., Carder, K. L. & Arnone, R. A. 2002 Deriving inherent optical properties from water color: a multiband quasi-analytical algorithm for optically deep waters. *Applied Optics* **41** (27), 5755–5772. doi:10.1364/AO.41.005755.

Lee, Z., Arnone, R., Hu, C., Werdell, P. J. & Lubac, B. 2010 Uncertainties of optical parameters and their propagations in an analytical ocean color inversion algorithm. *Applied Optics* **49** (3), 369–381. doi:10.1364/AO.49.000369.

Li, L., Li, L., Song, K., Li, Y., Tedesco, L. P., Shi, K. & Li, Z. 2013 An inversion model for deriving inherent optical properties of inland waters: establishment, validation and application. *Remote Sensing of Environment* **135**, 150–166. doi:10.1016/j.rse.2013.03.031.

Liang, W. J., Chun, X., Liu, J. Y., Xue, M., Siqin, B., Wu, Z. W. & Song, J. 2017 Research on the area change processes in the past 40a of Daihai Lake. *Journal of Arid Land Resources and Environment* **31** (4), 93–98.

Liang, X., Liu, H. M., Ji, M. C., Chang, M., Wen, L., Yu, R. H., Zhuo, Y. & Wang, L. X. 2021 Effects of land use/cover change on lake water quality in the semi-arid region of northern China: a case study in Lake Daihai Basin (2000–2018). *Journal of Lake Sciences* **33** (3), 727–736. doi:10.18307/2021.0309.

Liuzzo, L., Puleo, V., Nizza, S. & Freni, G. 2020 Parameterization of a Bayesian normalized difference water index for surface water detection. *Geosciences* **10** (7), 260. doi:10.3390/geosciences10070260.

Lorenzen, C. J. 1967 Determination of chlorophyll and pheo-pigments: spectrophotometric equations. *Limnology and Oceanography* **12**, 343–346. doi:10.4319/lo.1967.12.2.0343.

Ma, R., Tang, J. & Dai, J. 2006 Bio-optical model with optimal parameter suitable for Taihu Lake in water colour remote sensing. *International Journal of Remote Sensing* **27** (19), 4305–4328. doi:10.1080/01431160600857428.

McKinna, L. I. W., Fearns, P. R. C., Weeks, S. J., Werdell, P. J., Reichstetter, M., Franz, B. A., Shea, D. M. & Feldman, G. C. 2015 A semianalytical ocean color inversion algorithm with explicit water column depth and substrate reflectance parameterization. *Journal of Geophysical Research: Oceans* **120** (3), 1741–1770. doi:10.1002/2014JC010224.

Mishra, S., Mishra, D. R. & Lee, Z. P. 2014 Bio-optical inversion in highly turbid and cyanobacteria-dominated waters. *IEEE Transactions on Geoscience and Remote Sensing* **52** (1), 375–388. doi:10.1109/TGRS.2013.2240462.

Munnooru, K., Dash, S. K., Rao, G. D., Karri, R. & Rao, V. R. 2019 Estimation of inherent optical properties using quasi-analytical algorithm along the coastal waters of southeast Arabian Sea. *Ocean Dynamics* **69** (8), 925–937. doi:10.1007/s10236-019-01287-x.

Pitarch, J. & Vanhellemont, Q. 2021 The QAA-RGB: a universal three-band absorption and backscattering retrieval algorithm for high resolution satellite sensors. Development and implementation in ACOLITE. *Remote Sensing of Environment* **265**, 112667. doi:10.1016/j.rse.2021.112667.

Pitarch, J., Bellacicco, M., Organelli, E., Volpe, G., Colella, S., Vellucci, V. & Marullo, S. 2019 Retrieval of particulate backscattering using field and satellite radiometry: assessment of the QAA algorithm. *Remote Sensing* **12** (1), 77. doi:10.3390/rs12010077.

Pulliainen, J., Kallio, K., Eloheimo, K., Koponen, S., Servomaa, H., Hannonen, T., Tauriainen, S. & Hallikainen, M. 2001 A semi-operative approach to lake water quality retrieval from remote sensing data. *Science of the Total Environment* **268** (1–3), 79–93. doi:10.1016/S0048-9697(00)00687-2.

Shen, F., Zhou, Y. X., Li, D. J., Zhu, W. J. & Suhyb Salama, M. 2010 Medium resolution imaging spectrometer (MERIS) estimation of chlorophyll-*a* concentration in the turbid sediment-laden waters of the Changjiang (Yangtze) Estuary. *International Journal of Remote Sensing* **31** (17–18), 4635–4650. doi:10.1080/01431161.2010.485216.

Sun, D., Li, Y., Wang, Q., Le, C., Lv, H., Huang, C. & Gong, S. 2012 Specific inherent optical quantities of complex turbid inland waters, from the perspective of water classification. *Photochemical and Photobiological Sciences* **11** (8), 1299–1312. doi: 10.1039/C2PP25061F.

Tang, J. W., Tian, G. L., Wang, X. Y., Wang, X. M. & Song, Q. J. 2004 The methods of water spectra measurement and analysis I: above-water method. *Journal of Remote Sensing* **8** (1), 37–44.

Wang, Y., Liu, D. & Tang, D. 2016 Application of a generalized additive model (GAM) for estimating chlorophyll-*a* concentration from MODIS data in the Bohai and Yellow Seas, China. *International Journal of Remote Sensing* **38** (3), 639–661. doi:10.1080/01431161.2016.1268733.

Wang, Y., Shen, F., Sokoletsky, L. & Sun, X. 2017 Validation and calibration of QAA algorithm for CDOM absorption retrieval in the Changjiang (Yangtze) estuarine and coastal waters. *Remote Sensing* **9** (11), 1192. doi:10.3390/rs9111192.

Werdell, P. J., Franz, B. A., Bailey, S. W., Feldman, G. C., Boss, E., Brando, V. E., Dowell, M., Hirata, T., Lavender, S. J., Lee, Z., Loisel, H., Maritorena, S., Mélin, F., Moore, T. S., Smyth, T. J., Antoine, D., Devred, E., d'Andon, O. H. F. & Mangin, A. 2013 Generalized ocean color inversion model for retrieving marine inherent optical properties. *Applied Optics* **52** (10), 2019–2037. doi:10.1364/AO.52.002019.

Xi, B. D., Zhang, Y. L. & Xu, Q. J. 2012 Possibility of total dissolved solid as one of nutrient baselines in inner Mongolia-Xinjiang plateau. *Environmental Science* **33** (10), 3308–3313. doi:10.13227/j.hjkx.2012.10.020.

Yang, W., Matsushita, B., Chen, J., Yoshimura, K. & Fukushima, T. 2013 Retrieval of inherent optical properties for turbid inland waters from remote-sensing reflectance. *IEEE Transactions on Geoscience and Remote Sensing* **51** (6), 3761–3773. doi:10.1109/TGRS.2012.2220147.

Yentsch, C. S. & Menzel, D. W. 1963 A method for the determination of phytoplankton chlorophyll and phaeophytin by fluorescence. *Deep Sea Research* **10**, 221–231. doi:10.1016/0011-7471(63)90358-9.

Zeng, H. & Wu, J. 2010 Lake status of water quality and the changes in Inner Mongolia–Xinjiang Plateau. *Journal of Lake Sciences* **22** (6), 882–887. doi:10.18307/2010.0610.

Zhang, Y., Liu, M., Qin, B., van der Woerd, H. J., Li, J. & Li, Y. 2009 Modeling remote-sensing reflectance and retrieving chlorophyll-a concentration in extremely turbid case-2 waters (Lake Taihu, China). *IEEE Transactions on Geoscience and Remote Sensing* **47** (7), 1937–1948. doi:10.1109/TGRS.2008.2011892.

Zhou, Y. K., Jiang, J. H. & Huang, Q. 2006 Water quality analysis and assessment of Daihai Lake in Inner Mongolia. *Journal of Arid Land Resources and Environment* **20** (6), 74–77. doi:10.3969/j.issn.1003-7578.2006.06.014.

First received 24 May 2021; accepted in revised form 19 November 2021. Available online 7 December 2021